Egyptian Journal of Chemistry
http://ejchem.journals.ekb.eg/

Synthesis and Characterization of Polyaniline/Mn$_3$O$_4$/Reduced Graphene Oxide Nanocomposite

A.G. Darwish[1], A.M. Ghoneim[1], M.Y. Hassaan[2], O.S. Shehata[3], G. M. Turky[1]

[1]*Department of microwave Physics and Dielectrics, National Research Centre, Dokki, Giza, Egypt.*
[2]*Physics Division, Faculty of Science, El-azhar University, Cairo, Egypt*
[3]*Department of Physical Chemistry, National Research Centre, Dokki, Giza, Egypt.*

THE present work is concerned with the synthesis and studying the electrical and dielectric properties of Polyaniline (PANI)/Mn$_3$O$_4$/Reduced Graphene Oxide (RGO) nanocomposites using the Broadband Dielectric Spectroscopy technique. Polyaniline/Mn$_3$O$_4$ and polyaniline/Mn$_3$O$_4$/RGO nanocomposites were prepared using in-situ polymerization. To investigate the structural and morphology of the prepared samples, XRD, FTIR, HRTEM and SEM techniques were used. XRD results of pure Mn$_3$O$_4$ and PANI showed that PANI has crystallinity to some extent and the formation of Mn$_3$O$_4$ as a major phase with crystallite size ~20 nm is obtained. In case of nanocomposite samples, PANI/Mn$_3$O$_4$ and PANI /Mn$_3$O$_4$/RGO revealed a slight disappearance of the characteristic peaks of Mn$_3$O$_4$, which may be attributed to the covering of Mn$_3$O$_4$ surface by PANI. FTIR analysis of the nanocomposite samples indicated that the characteristic absorption peaks are shifted to higher wavenumbers compared with that of pure PANI confirming the interaction between PANI, graphene and Mn$_3$O$_4$. The morphological study of the samples revealed a porous surface of micro aggregates of Mn$_3$O$_4$ and PANI enveloped by RGO sheets and showed the distribution of Mn$_3$O$_4$ nanoparticle and PANI nanofibers on and between the thin sheets of RGO. The value of dc conductivity is rather high, and the prepared nanocomposites could be considered as synthetic metals from the conductivity point of view of such plastic electrode materials.

Keywords: Polyaniline, Manganese oxide, Reduced graphene oxide, Nanocomposites, Electrical conductivity

Introduction

The advance in material technology plays a substantial role in the development of electrical, industrial and energy storage materials. Conducting polymers are promising materials for the realization of high performance supercapacitors and sensor applications [1-4]. Polyaniline is considered as most convenient material because of its electrochemical characteristics, low cost, weather resistant, and facile synthesis. However, it suffers from low processability, inferior mechanical properties and poor stability during the charge/discharge process and it cannot be easily dissolved, which restricts its potential practical applications [3, 5, 6]. To overcome these drawbacks and enhance electrical and mechanical properties, PANI composites is formed with either carbon materials such as graphene or carbon nanotubes [5, 7, 8] or with metal oxides [6, 9] or with both [10, 11].Graphene, an atom-thick 2D nanostructure, has gained potential interest recently, wing to its great mechanical, thermal and electrical properties [12-14]. Using

graphene as a filler into polymer can fabricate prominent nanocomposites showing superior structural and functional properties compared to the neat polymer [15-18]. Manganese is one of the most abundant elements in the earth's crust. It has various oxidation states and structures [19, 20]. Recently, Mn_3O_4 is used in the manufacture of supercapacitors electrode [21]. The addition of Mn_3O_4 to the nanocmposite can achieve great stability to the charge- discharge process [22, 23].

The present study aims to synthesize a modified polyaniline and polyaniline nanocomposites polyaniline and polyaniline nanocomposites (PANI /RGO, PANI/ Mn_3O_4 and PANI/Mn_3O_4/RGO) by in-situ polymerization and to study the impact of Mn_3O_4 and graphene on the electrical properties of polyaniline. The structural and morphology properties of the synthesized samples were investigated using XRD, FTIR, HRTEM and SEM.

Experimental

Materials

Natural graphite powder was obtained from Merck, potassium permanganate from Sd Fine Chem, sodium nitrate from Acros Organics, manganese acetate and manganese nitrate tetra hydrate from Sigma Aldrich. Ammonia solution was obtained from Strem Chemicals, Aniline hydrochloride from Oxford Laboratory Reagents, Ammonium persulfate (APS) from Laboratory Rasayan, Sulphuric acid of 98% concentration and ethanol absolute from El Nasr pharmaceutical chemicals CO. Hydrogen peroxide (30% H_2O_2) and hydrochloric acid (35%) were obtained from Alpha Chemika, hydrazine hydrate from RANKEM laboratory reagents. All reagents were of analytical grade and were used as received.

Sample Preparation

A modified Hummer's method [24] was used to make graphene oxide (GO).

At first, 3.0 g of graphite and 1.5 g sodium nitrate were dissolved in 250 ml H_2SO_4 in an ice-bath and 9.0 g potassium permanganate were added slowly to the solution during stirring. Afterwards, it was stirred in water bath (35 °C) for 30 min. Then, 250 ml deionized water was advisedly added to the solution, and the solution temperature was kept at 98 °C for 30 min. In order to terminate the reaction 300 ml deionized water and 60 ml of hydrogen peroxide was added. The solution's color transformed to dark yellow. The produced solution was filtered then the solid obtained washed with

distilled water for several times. Graphene oxide powder was obtained by centrifugation then drying at 60 °C for 12 h. Finally, RGO was obtained by the reduction of graphene oxide. Graphene oxide suspension (0.5g GO in 50 ml H_2O) was added to 4 ml of hydrazine hydrate and 3 ml of ammonia solution (30%) in a 250 ml flask then washing with distilled water to remove the excess hydrazine and finally dried overnight.

Trimanganese Tetraoxide Mn_3O_4 was prepared

by a sol–gel technique using citric acid as a chelating agent [20]**.** First 7.53 g of manganese nitrate was dissolved into a mixed solution of 20 ml distilled water and 10 ml ethanol, and then citric acid was added under stirring. The solution was kept under stirring for 4 h and then the produced gel was dried at 80 °C overnight, and finally calcined at 400 °C for 4 h. For the preparation of Mn_3O_4/RGO, the same steps for preparing Mn_3O_4 were followed with one modification, RGO suspension (0.2 g in 20 ml H_2O) was ultrasonicated for 30 minutes and then added to the manganese nitrate/citric acid solution during stirring.

The preparation of PANI and its nanocomposites: PANI was prepared as given by Zou et al [26].

Aniline hydrochloride and APS were dissolved separately in 1.0 M HCl (0.2 M and 0.25 M, respectively) and kept stirring for about 30 min. APS solution was then added to the Aniline hydrochloride solution. The flask was covered and left under stirring overnight. The obtained solution was filtrated then washed with distilled water and then dried at 70 °C for 48 h. For the nanocomposites preparation, the fillers (RGO or Mn_3O_4 or both) are added firstly to the aniline monomer during stirring, then after 4 h of vigorous stirring APS was added to the solution. Then the mixture solution was undergone 24 h vigorous stirring and then separated out by filtration, washed by distilled water and dried at 70 °C for 48 h. The prepared doped samples were PANI/Mn_3O_4 (50:50 wt%) and PANI/Mn_3O_4/ RGO (47.5:47.5:5 wt%) .

Characterization Techniques:

The crystallographic structures of the materials were determined by a powder X-ray diffraction system (XRD) [Bruker D8 Advance diffractometer] equipped with Cu Kα radiation (k = 0.15406 nm) operating at 40 kV and 40 mA. The XRD patterns were collected in the range 4 - 80° at

a scan rate of 0.02°/min. The molecular structure of the prepared hybrids was analyzed using a (Nicolet Magma 550 series II, Midac, USA) at wavelengths ranging from 4000 to 400 cm⁻¹. The powder was grounded with KBr powder and compressed into discs for FTIR examination. The microstructure of the samples was investigated by JEOL (Japan) JSM-T300 scanning electron microscope (SEM) and with a high-resolution transmission electron microscope (HRTEM, FEI Philips Tecnai G2 S-Twin operated at 200 keV). The dielectric measurements were carried out by means of a Novocontrol high resolution alpha dielectric analyzer in the frequency range 0. 1 Hz to 10 MHz. The analyzer was supported by Quatro temperature controller using pure nitrogen as heating agent and providing temperature stability better than 0.2 K. The dielectric measurements were conducted, using gold-plated Brass electrodes of 10 mm in diameter, in parallel plate capacitor configuration.

Results and Discussion

X-ray diffraction (xrd) studies:

Figure 1 shows the XRD patterns of RGO and graphene oxide. Graphene oxide (GO) has a clear peak centered at $2\theta = 10.91°$, that correspond to the (002) reflection of piled up graphene oxide sheets [24]. The interlayer spacing of the used graphite and the prepared GO were 0.336 and 0.7984 nm, respectively. The change in the interlayer spacing indicates the presence of some oxygen containing groups on graphene oxide sheets due to the oxidation and implying the exfoliation of graphite [24-25]. After chemical reduction by hydrazine, the sharp (002) peak of graphene oxide is shifted to $2\theta \approx 24°$ and became broader, implying a disorder in the reduced graphene sheets. The change in the interlayer spacing d_{002} from 0.7984 nm for graphene oxide to 0.3746 nm for RGO suggests the exfoliation of graphene oxide sheets [24]. Moreover, the d-spacing RGO is greater than that of graphite indicating the presence of some oxygenated residuals [25].

The XRD pattern of Mn_3O_4 is given in Fig.2. It is clarified the formation of nano Mn_3O_4 as an essential phase. All the peaks can be indexed with those reported in the literature for Mn_3O_4 (JCPDS card no 24-0734) [27]. The diffraction peaks at $2\Theta = 18.3, 28.9, 32.3, 36.2, 38$ and $59.9°$ can be indexed as the diffraction planes (101), (112), (103), (211), (004) and (224), respectively. The crystallite size calculated from (211) peak broadening using the Scherrer's formula [28] was found to be ~20 nm.
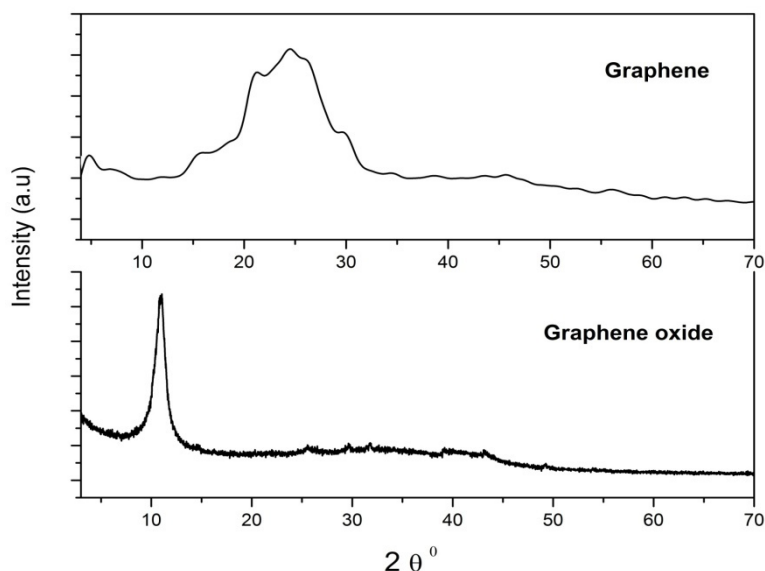

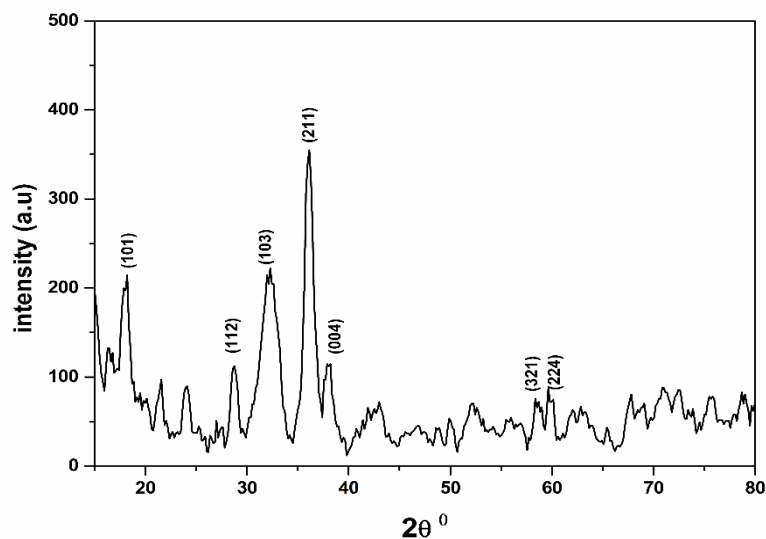**Fig. 1: XRD pattern of graphene and graphene oxide.**

Fig. 2: XRD pattern of Mn$_3$O$_4$.

Figure 3 provides the XRD patterns of polyaniline (PANI), polyaniline/Mn$_3$O$_4$ and polyaniline/Mn$_3$O$_4$/RGO nanocomposites. From this figure, pure PANI exhibits a diffraction peak at $2\Theta = 25.8°$ attributing to the plane (021) (JCPDS 53-1891) [28], indicating that PANI has a crystallinity to some extent. This crystallinity may be attributed to the duplication of benzenoid and quinoid rings in PANI chains [28].The characteristic peaks of Mn$_3$O$_4$ almost disappeared in the XRD patterns of PANI/Mn$_3$O$_4$ and PANI/ Mn$_3$O$_4$/RGO, which may be due to the covering of the surface of Mn$_3$O$_4$ by PANI. In addition, the existence of graphene restricts the growth of the crystal planes. The peaks found at about 18° and 36° are indexed to Mn$_3$O$_4$ which attributed to (101) and (211) diffraction planes, respectively, according to JCPDS card # (24-0734) [27].
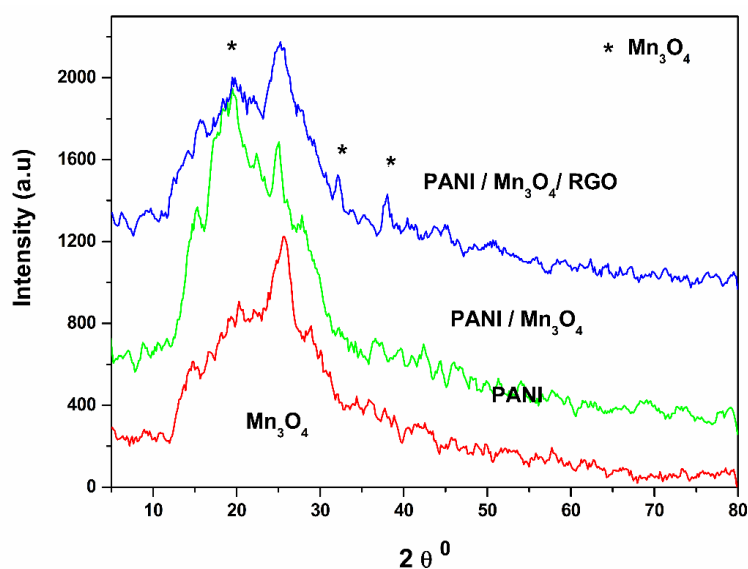

Fig. 3: XRD patterns of PANI, PANI/Mn$_3$O$_4$ and PANI/Mn$_3$O$_4$/RGO nanocomposites.

Fourier transforms infrared (ftir) analysis:

Figure (4) presents the FTIR spectra of Mn_3O_4 and Mn_3O_4/ RGO nanocomposite. The vibration frequency at 606 cm^{-1} is the characteristic of Mn–O stretching modes in tetrahedral sites, whereas vibration frequency at 491 cm^{-1} corresponded to the Mn–O distortion vibration [20]. The weak vibration band, appeared at a lower wave number (433 cm^{-1}), could be attributed to the vibration of manganese ion (Mn^{3+}) in octahedral sites. It faded in case of graphene doped sample. The peaks at 1382 cm^{-1} and 1118 cm^{-1} are attributed to NO_3^- related stretching vibration. This revealed that a trace amount of NO_3^- related materials was bonded to the surface of Mn_3O_4. While, the bands at 2921 and 2853 cm-1 are due to organic residues originating from the sample as a result of the preparation procedure. Finally, both of the broad band at 3425 cm^{-1} and the weak band at 1627 cm^{-1} were observed due to the absorbed and physically adsorbed water, which were attributed to stretching and bending vibrations of water molecules.
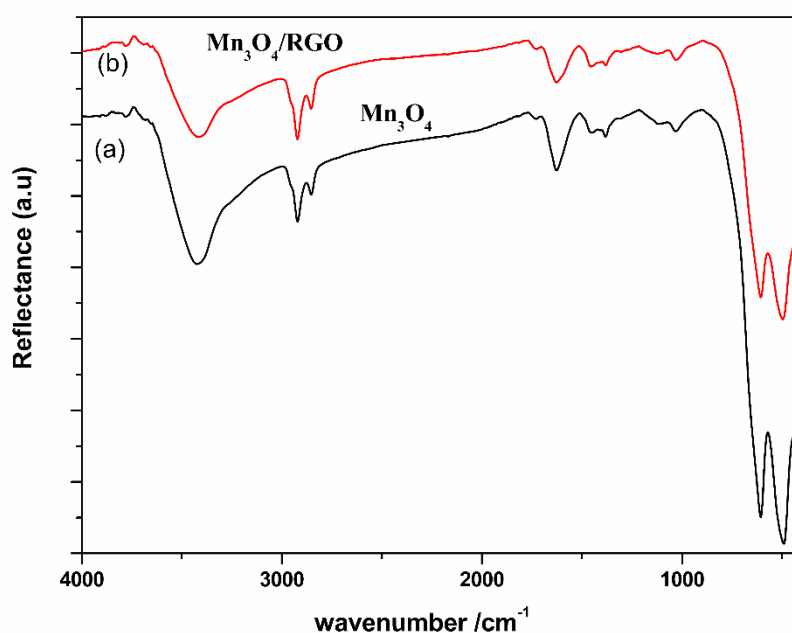

Fig. 4: FTIR spectra of (a) pure Mn_3O_4 and (b) Mn_3O_4/RGO annealed at 400 ºC.

The FTIR spectra of pure PANI, PANI/Mn_3O_4, PANI/RGO and PANI/Mn_3O_4/RGO nanocomposites are shown in figure 5. For pure PANI, the characteristic peaks at 1581 and 1464 cm^{-1} can be designated to the C - C stretching vibration of quinoid ring and benzenoid ring, respectively [29].The band at 1298 cm^{-1} originates from the C—N stretching of the secondary aromatic amine. The band at 1125 cm^{-1} is attributed to the C—H in-plane bending mode. The bands at 801 and 877 cm^{-1} originate from the out of plane bending vibration for C—H, which agree well with the emeraldine salt form of PANI [29]. Also the FTIR spectrum shows high wavenumber bands correspond to N—H stretching (3430 cm^{-1}) and aromatic C—H stretching (2923 cm^{-1}) [29, 30].

For PANI/RGO sample, the characteristic absorption peak corresponding to PANI at 1464 cm^{-1} in PANI/ RGO shifts to higher wavenumbers compared with pure PANI This shift may be attributed to the interactions between the PANI and graphene. For PANI/Mn_3O_4 and PANI/Mn_3O_4/graphene samples, the band in the region from 400 to 800 cm^{-1} can be assigned to Mn—O stretching vibrations [31].

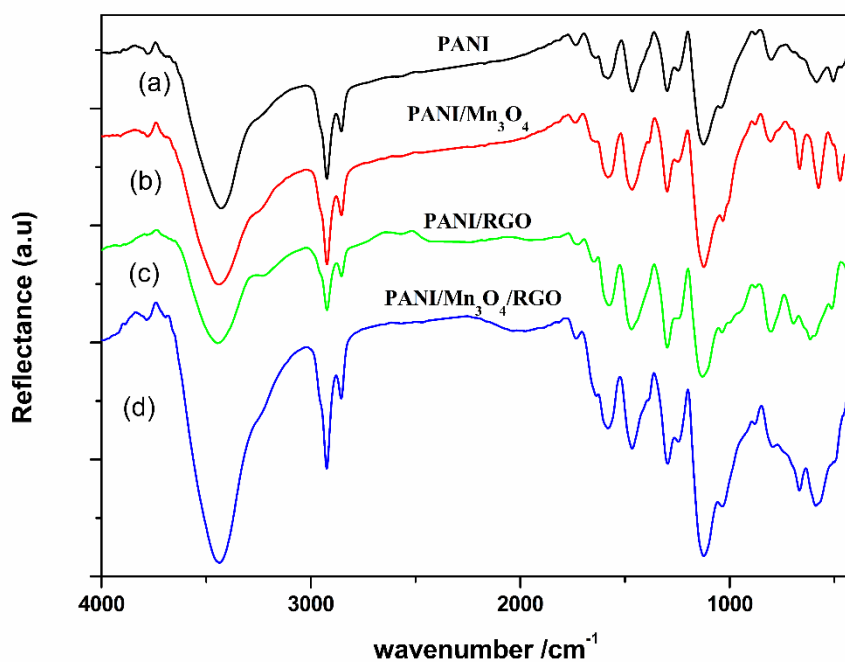**Fig. 5: FTIR of PANI, PANI/Mn$_3$O$_4$, PANI/RGO and PANI/Mn$_3$O$_4$/RGO.**

Uv-vis spectra of pani and pani nanocmposites

The UV-vis spectra of the different samples are shown in figure 6. UV-vis spectra represent the characteristic peaks of the emeraldine oxidation state of polyaniline. The spectra show three bands at 351, 458 and 877 nm. The first peak is due to

the n-π* transition, the second is attributed to π-π* transition of the aromatic rings, while the third is associated with the charge carried in the polymer chain. For PANI/Mn$_3$O$_4$/RGO nanocomposites in Fig. 6(c), the spectrum declared that no transitions take place.
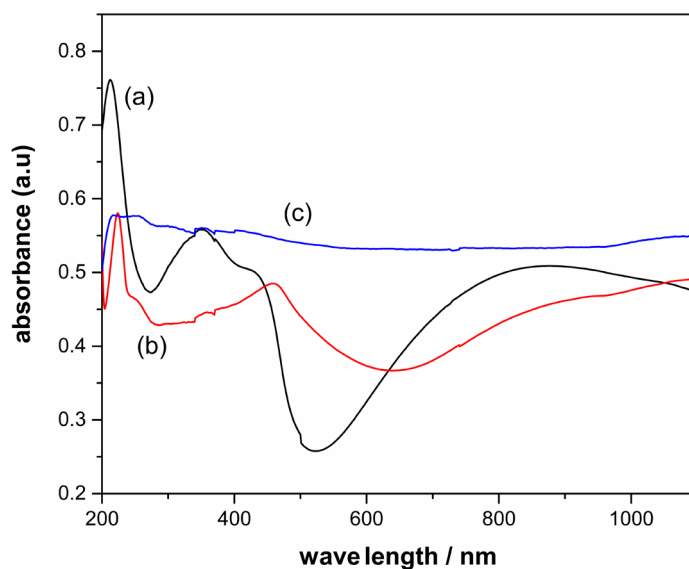

Fig. 6: UV-Vis spectra for PANI (a), PANI/Mn$_3$O$_4$ (b) and PANI/Mn$_3$O$_4$/RGO (c) nanocomposites.
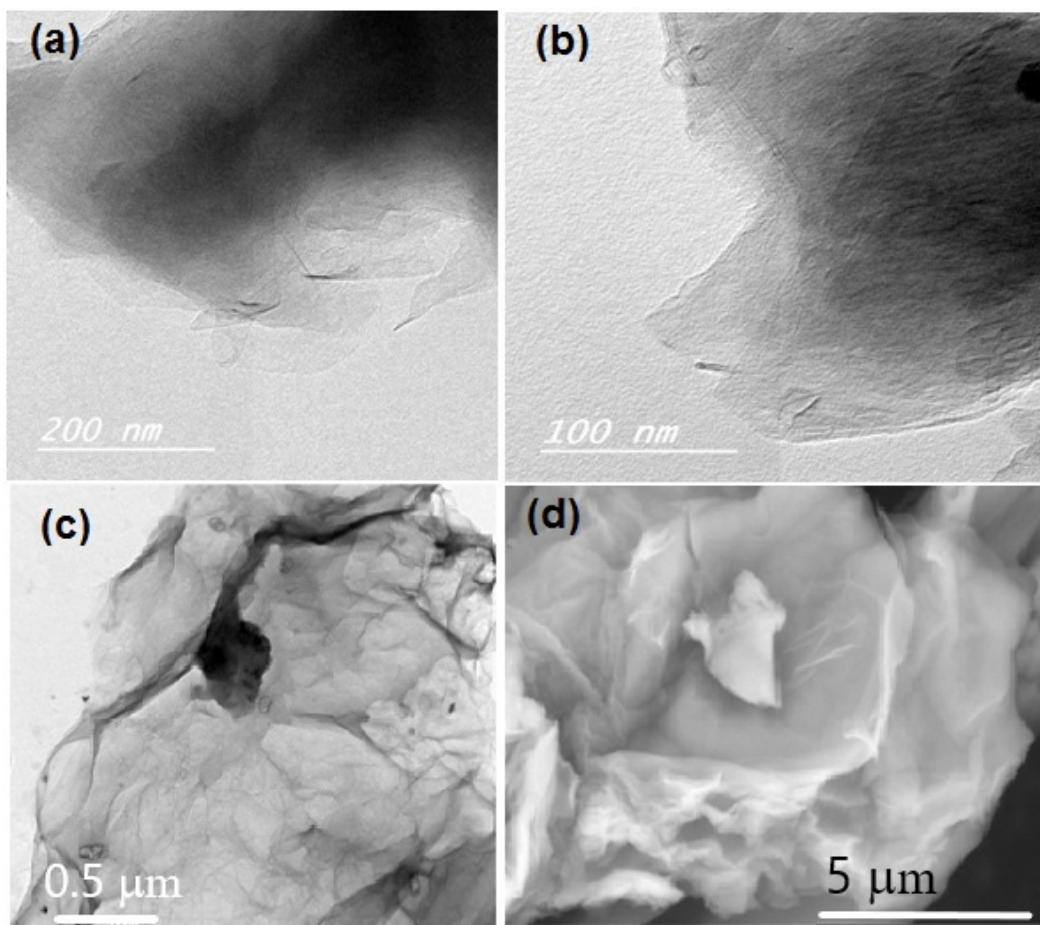
Fig. 7: HRTEM (a and b) TEM (c) and SEM (d) of RGO.3.4 Morphological Analysis:

The morphology of the prepared samples is studied using HRTEM and SEM. The micrographs for graphene is illustrated in figure 7. The typical entangled, thin, crumpled and wrinkled texture of graphene sheets can be seen in this figure. It is clear that the produced RGO sheets are few layers thick and highly transparent.

Figure 8 shows the HRTEM image of Mn_3O_4. It displays like fused large particles with rough surfaces. The size of Mn_3O_4 particles is ranged between 30–80 nm.

Figure 9 shows SEM and HRTEM images of Pure PANI at different magnifications. SEM images (9a and b) show aggregations of fibrous structure. HRTEM illustrates the morphology and structure of these aggregations. HRTEM for pure PANI shows a rod-like fibrous shape with thickness about 50 nm and with different lengths. These fibrous nanorods cross-link with each other

forming three-dimensional networks, which will facilitate the transfer of electrons.

The morphology of PANI/RGO nanocomposite at RGO concentration of 10 wt% is shown in Fig. 10 a. It is revealed that graphene sheets encapsulate PANI. Figure 10b and c shows SEM images of PANI/Mn_3O_4 at different magnifications. It exhibits an evidently aggregated structure of smaller granules of Mn_3O_4 with rough porous surface of dense agglomeration within the PANI.

The images of PANI/Mn_3O_4/RGO composites in the figure 10d, e and f revealed a porous surface of micro aggregates of Mn_3O_4 and PANI enveloped by thin film of graphene with a large surface area. HRTEM image showed the distribution of nanoparticle of Mn_3O_4 and PANI nanofibers on and between the thin sheets of RGO (Fig. 10f). The intimate contact between graphene sheets,

PANI and Mn_3O_4 can be clearly observed from both SEM and TEM images, which is important for improving electrical conductivity.
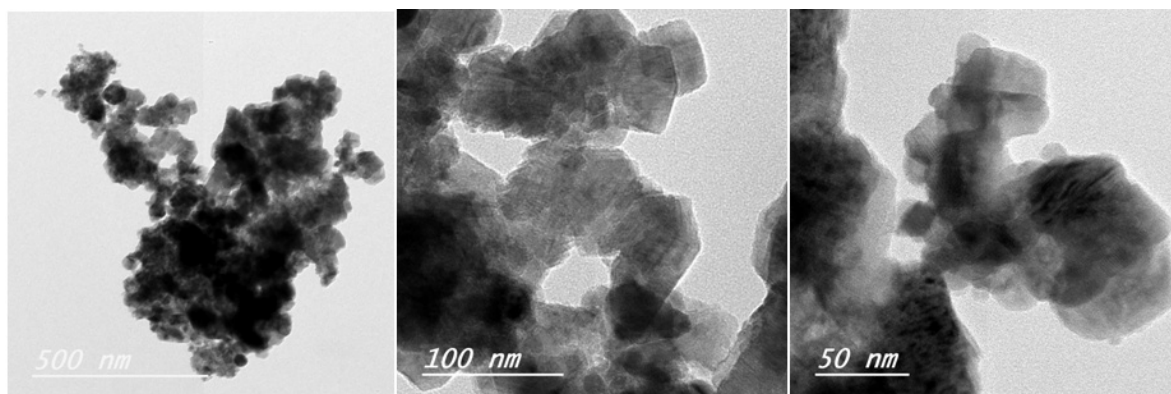

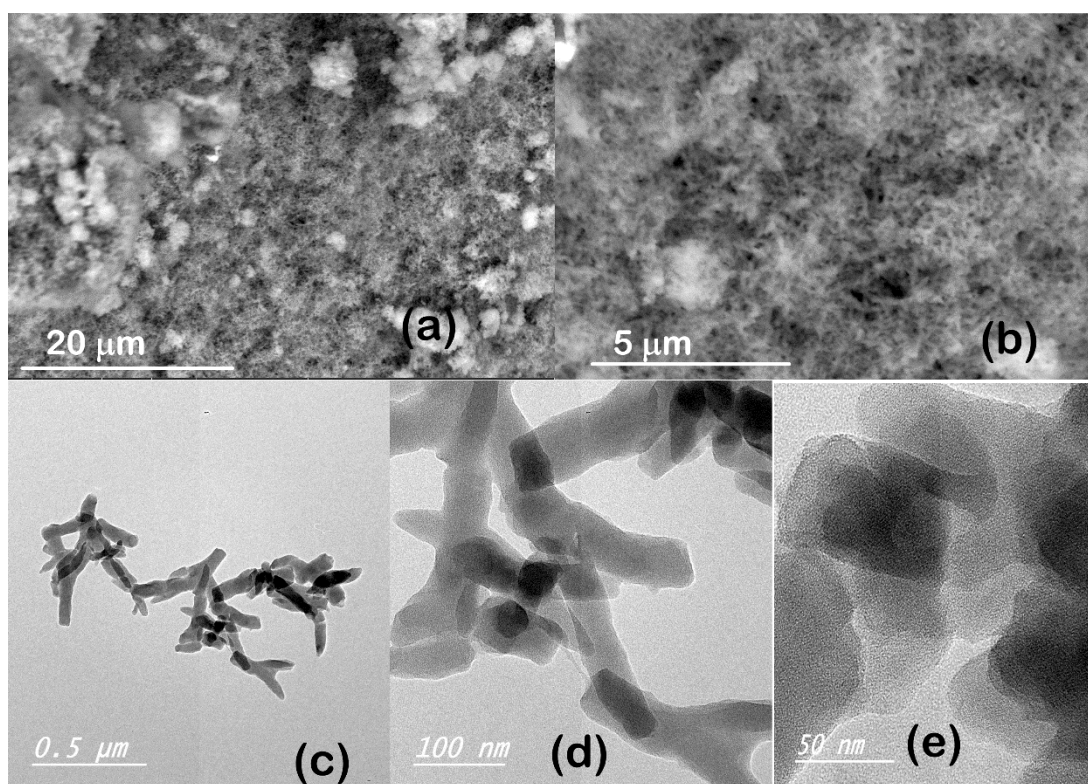**Fig. 8: The HRTEM of Mn_3O_4 at different magnifications.**

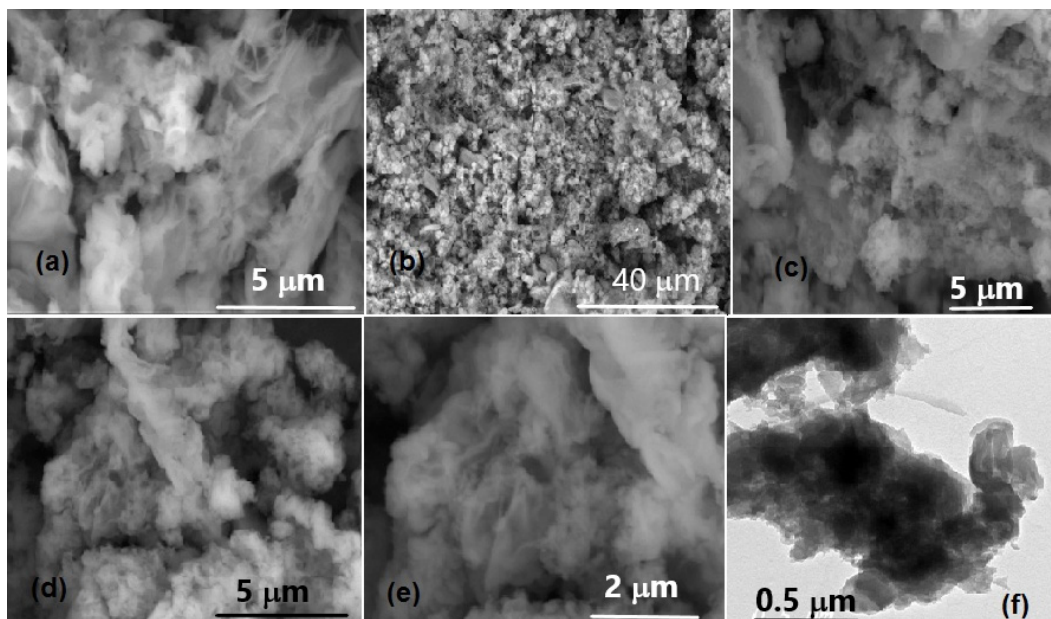**Fig 9: SEM (a and b) and HRTEM (c, d and e) images of Pure PANI at different magnifications.**

Fig. 10: SEM of PANI/graphene (a), PANI/ Mn_3O_4 (b and c) and PANI/ Mn_3O_4/ RGO (d and e) and HRTEM of PANI/ Mn_3O_4/ RGO (f).

Dielectric and electrical properties

The Dielectric and electrical properties of the prepared PANI was measured on the frequency range 0.1 - 10MHz and temperatures ranging from -50 up to 150 °C. The complex dielectrics function, whereis the permittivity and is the dielectric loss, which obtained in the frequency range 10^{-1}-10^7 Hz and at temperatures ranging from 273 K to 423 K with scan rate 10 K. It is equivalent with the complex conductivity function since,, implying that and (being the vacuum permittivity)

The imaginary part of the complex permittivity, ε'', is illustrated graphically against frequency at some selected temperatures ranging between 40 and 130 °C (figure 11). It is clear from this figure that: I) the dielectric loss, ε'', values increased gradually with decreasing frequency and reached extra high values at lower frequencies II) there is no relaxation peaks could be seen, III) the effect of temperature is negatively affected the dielectric loss, in other words the high the temperature the lower the dielectric loss.
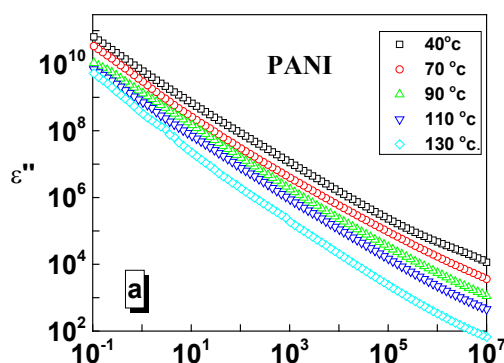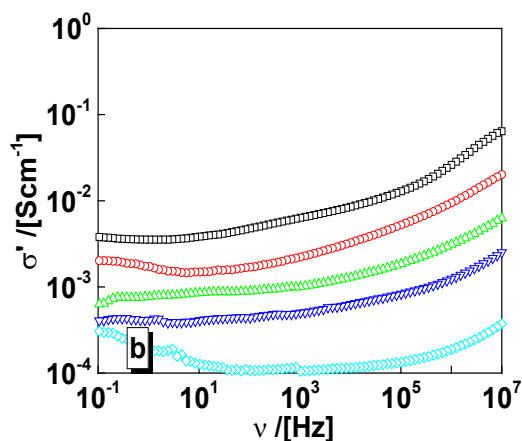
Fig. 11: The imaginary part of complex permittivity ε" (a)and real part of the complex conductivity σ'(b) of the prepared polyanilene at different temperatures as given in the legends.

This behavior is somewhat abnormal and unexpected in such conductive polymers. Figure 11b represents the real part of the complex conductivity versus frequency at the same temperatures as given in figure 11a. Once again, the temperature inversely affected the conductivity. Generally, it can be noticed also that the values of the conductivity of PANI is much higher than that of the ceramics.

The dielectric loss, ε", and real conductivity, σ', of the 50 wt% Mn_3O_4 doped in PANI were measured at temperatures varied from -50 up to 150 °C. The data are represented in figure 12a and b at some selected temperatures and over the range of frequency from 0.1 Hz to 10 MHz. The effect of frequency in decreasing the ε" values is very high and reached about 7 to 8 decades. The linear relation here have ignored any effect of molecular dynamic relaxations since there is no dielectric relaxation peaks could be seen here. Anomalous effect of temperature is noticed here, that is no systematic influence on the values of ε" could be seen here but ε" increased by increasing temperature till about 70 °C, then further increase of temperatures decreases ε". Is there some inflection point here?? And if so, how could we interpret this unexpected behavior?

The real part of the complex conductivity, σ', is illustrated versus frequency at the same temperatures (Figure 11b). Similar effect of temperature on the dc - conductivity (that is the values of the σ' at the independent range of frequency) could be seen here.

The conductivity values are very high and there is some indication of the development of the electrode polarization that decreases gradually σ' values at lower frequencies due to the accumulation of the charge carriers at the interface between the metal electrode (Brass) and the polymer nanomposite materials under consideration.

Figures (11) and (12) indicate that PANI and its considered nanocomposites behave like many other conductive disordered materials like ionic liquids, conductive glasses ...etc. That is at higher temperatures (and lower frequencies) the dielectric spectra are dominated by charge transport (evident from the plateau value of σ' or slope of -1 in the dielectric loss, ε") and electrode polarization

Figure (13) shows σ' against frequency at some considered temperatures for the three component polymer nanocomposite, PANI/Mn_3O_4/ RGO (50:45:5 wt %). This illustration accompanied by the dielectric loss (see for instance figure 13) independent of frequency may clarify that the dielectric response here is mainly or only due to the migration of charge carriers rather than the molecular fluctuations. At lower frequencies, the electrode polarization starts to develop especially at higher temperatures.

It is very interesting to notice that the values of dc conductivity is rather high and the prepared nanocomposites could be considered as synthetic metals from the conductivity point of view of such plastic electrode materials. This is the main
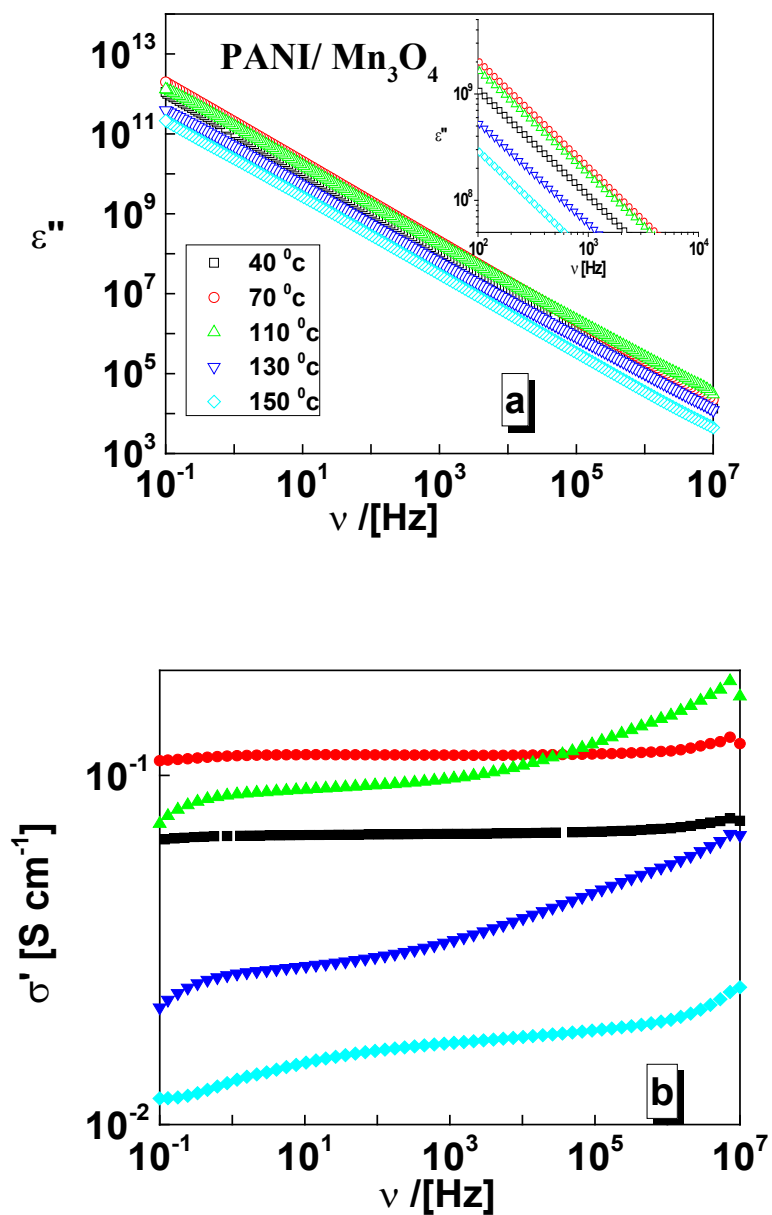
goal of the present work.

Fig. 12: The imaginary part of complex permittivity ε"(a) and real part of the complex conductivity σ' (b) of the PANI/Mn$_3$O$_4$ (50:50 wt%) at different temperatures as given in the legends. The inset of a is rescaling of the data.
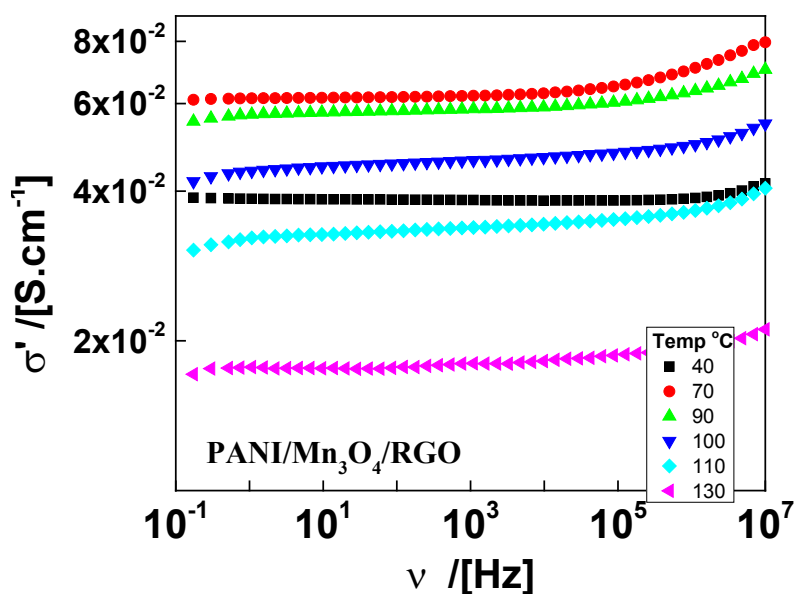
Fig. 13: The real part of the complex conductivity, σ', of the PANI/Mn₃O₄/ RGO at different temperatures as given in the legends.

The dc-conductivity σ_{dc} as well as the dielectric loss ε'' at spot frequency point 1 kHz deduced for PANI/Mn₃O₄/RGO nanocomposite are illustrated graphically versus temperatures in figure 14a and b), respectively. It is clear from the figure that the adsorbed and absorbed moisture plays a very important role in the transportation of the charge carriers. That is both parameters increases gradually with increasing temperatures due to the increasing of the mobility which reduces dramatically the calorimetric glass transition. This

is due to the well known plasticizing effect of the moisture in such polymeric nanocomposites.

The anomalous behavior of dc conductivity according to the moisture is accompanied by similar inflection point of the dielectric loss is shown in figure 14b. This similar behavior of both parameters again assures that the dielectric response is due to the transportation of charge carriers reflecting by the conductivity but not the dielectric relaxation peaks.
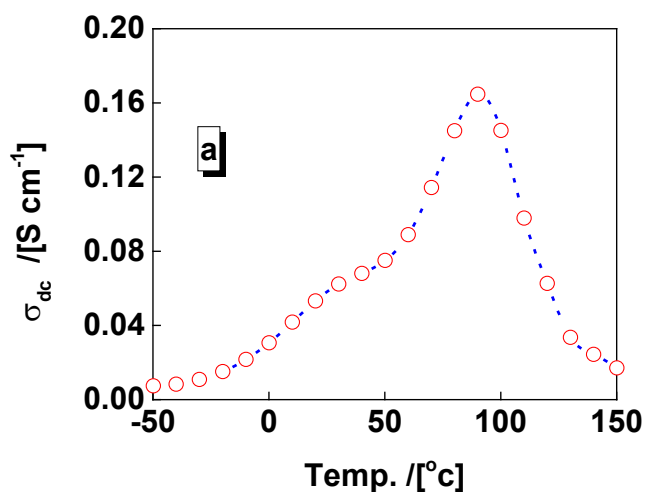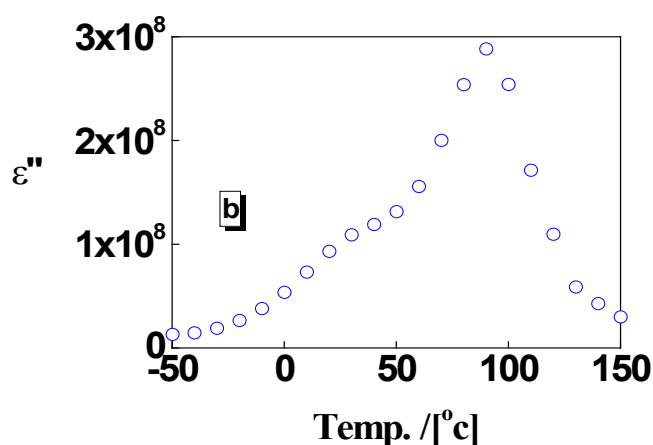
Fig. 14: σ_{dc} (a) and ε" (b) at 1 kHz for the PANI/Mn$_3$O$_4$/RGO nanocomposite against temperatures

Conclusions

Pure polyaniline and polyaniline nanocomposites were prepared by insitue polymerization. .XRD pattern of Mn$_3$O$_4$ indicates the formation of Mn$_3$O$_4$ as the major phase with crystallite size ~20 nm .XRD patterns of PANI shows its crystallinity to some extent. XRD patterns of PANI/Mn$_3$O$_4$ and PANI/Mn$_3$O$_4$/RGO reveals a slight disappearance of the characteristic peaks of Mn$_3$O$_4$.The morphological study of the samples shows that Mn$_3$O$_4$ has fused large particles with rough surface. For polyaniline it shows a rod-like fibrillar structure cross-linking with each other. The nanocomposite samples revealed a porous surface of micro aggregates of Mn$_3$O$_4$ and PANI enveloped by thin film of graphene with a large surface area.

The values of dc conductivity is rather high and the prepared nanocomposites. The prepared nanocomposites could be considered as synthetic metals from the conductivity point of view of such plastic electrode materials. However, the adsorbed and absorbed moisture plays a very important role in the transportation of the charge carriers. Both parameters (σ' and ε'') increase gradually with increasing temperatures. This was attributed to the increase of the mobility of charge carriers which reduces dramatically the calorimetric glass transition.

References

1. Ahad I.Z.M., Harun S.W., Gan S.N., Phang S.W., Polyaniline (PAni) optical sensor in chloroform detection. *Sensors and Actuators B: Chemical* **261**, 97-105 (2018).

2. Lee C.T., Wang Y.S., High-performance room temperature NH$_3$ gas sensors based on polyaniline-RGO nanocomposite sensitive membrane. *Journal of Alloys and Compounds*, **789,** 693-696(2019).

3. Lee K.U, Byun J.Y., Shin H.J., Kim S.H., A high-performance supercapacitor based on polyaniline-nanoporous gold. *Journal of Alloys and Compounds*, **779**, 74-80(2019)

4. Wu X., Lian M., Highly flexible solid-state supercapacitor based on graphene/ polypyrrole hydrogel. *Journal of Power Sources,* **362**, 184-191(2017). 5- Li K., Liu X., Chen S., Pan W., Zhang J., A flexible solid-state supercapacitor based on graphene/polyaniline paper electrodes. *Journal of Energy Chemistry***, 32**,166-173(2019).

5. Elahi A., Irfan M., Shakoor A., Niaz N.A., Mahmood K., Qasim M., Effect of loading titanium dioxide on structural, electrical and mechanical properties of Polyaniline nanocomposites. *Journal of Alloys and Compounds*, **651,** 328–332 (2015).

6. Ladrón-de-Guevara A., Boscá A., Pedrós J., Climent-Pascual E., de Andrésc A., Calle F., Martínez J., RGO/polyaniline electrochemical supercapacitors fabricated by laser. *Applied*

Surface Science, **467–468**, 691-697(2019).

7. Mensing J. P., Lomas T., Tuantranont A., Ammonia strengthened graphene/CNT-wrapped polyaniline-nanofiber composites loaded with palladium nanoparticles for coin cell Supercapacitors. *Electrochimica Acta*, **263**, 17-25 (2018).

8. Vidya J., Balamurugan P., Synthesis, Structural, Morphological and Optical Characterization of Polyaniline hydrochloride/Cerium Oxide Nanocomposite. *Materials Today: Proceedings*, **8(1)**, 223-230 (2019).

9. Viswanathan A., Prakashaiah B. G., Subburaj V., Shetty A. N., High energy RGO/vanadium Pentoxide/polyaniline hybrid supercapacitor for power backup and switched capacitor converters. *Journal of Colloid and Interface Science*, **545**, 82-93 (2019).

10. Yang Z., Qiu A., Ma J., Chen M., Conducting α-Fe_2O_3 nanorod/polyaniline/CNT gel framework for high performance anodes towards Supercapacitors. *Composites Science and Technology*, **156**, 231-237 (2018).

11. Cao Y., Li G., Li X., Graphene/layered double hydroxide nanocomposite: Properties, synthesis, and applications. Chemical Engineering Journal, **292**, 207-223 (2016).

12. Srivastava V., Jain K., At room temperature graphene/SnO_2 is better than MWCNT/SnO_2 as NO_2 gas sensor *Materials Letters*, **169**, 28-32 (2016).

13. Kordatos A., Kelaidis N., Giamini S. A., Velasco J. M., Xenogiannopoulou E., Tsipas P., Kordas G., Dimoulas A., AB stacked few layer graphene growth by chemical vapor deposition on single crystal Rh(1 1 1) and electronic structure characterization. *Applied Surface Science*, **369**, 251-256 (2016).

14. Gupta S., McDonald B., Carrizosa S.B., Price C., Microstructure, residual stress, and intermolecular force distribution maps of graphene/polymer hybrid composites: Nanoscale morphology-

promoted synergistic effects. *Composites Part B: Engineering*, **92**, 175-192 (2016).

15. Jin Y., Huang G., Han D., Song P., Tang W., Bao J., Li R., Liu Y., Functionalizing graphene decorated with phosphorus-nitrogen containing dendrimer for high-performance polymer nanocomposites. *Composites Part A: Applied Science and Manufacturing*, **86**, 9-18 (2016).

16. Zhao Y.H., Zhang Y.F., Bai S.L., High thermal conductivity of flexible polymer composites due to synergistic effect of multilayer graphene flakes and graphene foam. *Composites Part A: Applied Science and Manufacturing*, **85**, 148-155 (2016).

17. Alizadeh T., Azizi S., Graphene/graphite paste electrode incorporated with molecularly imprinted polymer nanoparticles as a novel sensor for differential pulse voltammetry determination of fluoxetine. *Biosensors and Bioelectronics*, **81**, 198-206 (2016).

18. Wang L., Li Y., Han Z., Chen L., Qian B., Jiang X., Pintoc J., Yang G., Composite structure and properties of Mn_3O_4/graphene oxide and Mn_3O_4/graphene. *Journal of Materials Chemistry A*, **1**, 8385-8397 (2013).

19. Rani B.J., Ravina M., Ravi G., Ravichandran S., Ganesh V., Yuvakkumar R., Synthesis and characterization of hausmannite (Mn_3O_4) nanostructures. *Surfaces and Interfaces*, **11**, 28-36 (2018).

20. Luo Y., Yang T., Li Z., Xiao B., Zhang M., High performance of Mn_3O_4 cubes for supercapacitor applications.*Materials Letters* **178**, 171–174 (2016). 22- Liu H., Xue Q., Zhao J., Zhang Q., Enhanced supercapacitive performance of binary cooperative complementary $Co(OH)_2$/Mn_3O_4 nanomaterials directly synthesized through ion diffusion method controlled by ion exchange membrane *Electrochimica Acta,* **260,** 330-337 (2018).

21. Ren Y., Wang J., Huang X., Ding J., The synthesis of polypyrrole @ Mn_3O_4/RGO anode with improved coulombic efficiency. *Electrochimica*

Acta, **186**, 345-352(2015).

22. Muzyka R., Kwoka M., Smędowski L., Díez N., Gryglewicz G., Oxidation of graphite by different modified Hummers methods. *New Carbon Materials*, **32**, 15-20 (2017).

23. Yoo M.J., Park H.B., Effect of hydrogen peroxide on properties of graphene oxide in Hummers method. *Carbon*, **141**, 515-522 (2019).

24. Zou Y., Wang Q., Xiang C., Tang C.,Chu H., Qiu S., Yan E., Xu F., Sun L., Doping composite of polyaniline and reduced graphene oxide with palladium nanoparticles for room-temperature hydrogen-gas sensing. *International Journal of Hydrogen Energy*, **41(11)**, 5396-5404 (2016).

25. Raj B. G. S., Asiri A. M., Wu J. J., Anandan S., Synthesis of Mn_3O_4 nanoparticles via chemical precipitation approachfor supercapacitor application, *Journal of Alloys and Compounds,* **636**, 234-240 (2015)

26. Parra M.R., Haque F.Z., Aqueous chemical route synthesis and the effect of calcination temperature on the structural and optical properties of ZnO nanoparticles. *Journal of Materials Research and Technology*, **3**, 363-369 (2014).

27. Das M., Akbar A., Sarkar D., Investigation on dielectric properties of polyaniline (PANI) sulphonic acid (SA) composites prepared by interfacial polymerization. *Synthetic Metals*, **249**, 69-80 (2019)

28. Cong H.P., Ren X.C., Wang P., Yu S.H., Flexible graphene–polyaniline composite paper for high-performance supercapacitor. *Energy & Environmental Science*, **6**, 1185–1191 (2013).

29. Chen W., Tao X., Li Y., Wang H., Wei D., Ban C., Hydrothermal synthesis of graphene-MnO_2-polyaniline composite and its electrochemical performance. *Journal of Materials Science: Materials in Electronics*, **27**,6816–6822 (2016) .